Applied Geochemistry 155 (2023) 105729

Contents lists available at ScienceDirect

Applied Geochemistry

journal homepage: www.elsevier.com/locate/apgeochem

Effects of long-distance transport on O_3 and secondary inorganic aerosols formation in Qingdao, China

Yu Yang [a], Liubin Huang [a,*], Yingnan Zhang [d], Yuhong Liu [c], Yue Sun [a], Xiong Tuo [a], Yan Zhang [a], He Meng [b], Yujiao Zhu [a], Lingxiao Yang [a], Wenxing Wang [a], Likun Xue [a,**]

[a] Environment Research Institute, Shandong University, Qingdao, 266237, China
[b] Qingdao Eco-environment Monitoring Center of Shandong Province, Qingdao, 266003, China
[c] Key Laboratory of Marine Environment and Ecology, Frontiers Science Center for Deep Ocean Multispheres and Earth System, Ministry of Education, Ocean University of China, Qingdao, 266100, China
[d] Department of Civil and Environmental Engineering, Hong Kong Polytechnic University, Hong Kong, China

ARTICLE INFO

Editorial handling by Shengrui Tong

Keywords:
Field observation
Ozone
Secondary inorganic aerosols
Lagrangian photochemical trajectory model
Regional transport

ABSTRACT

This work presents a three-year continuous observation of ozone (O_3) and fine particle ($PM_{2.5}$), as well as their precursors in Qingdao, China, from September 2018 to August 2021. The annual concentrations of O_3 and $PM_{2.5}$ were measured as 35.9–44.5 ppbv and 31.6–34.2 μg m^{-3}, respectively. Analysis of the interannual variations of O_3 and $PM_{2.5}$ concentration indicated the effective control measures for $PM_{2.5}$ and O_3 pollution in Qingdao in recent years. Nevertheless, we still observed 85 O_3 episodes and 80 $PM_{2.5}$ episodes during the whole observation. And it was found that the fraction of secondary inorganic aerosols (SIA) in $PM_{2.5}$ mass significantly increased during $PM_{2.5}$ episodes. By employing the Lagrangian photochemical trajectory model (LPTM), we investigated the roles of local production and regional transport (i.e., short-distance transport and long-distance transport) that play in the O_3 and SIA formation in these episodes. The contribution of local production, short-distance transport, and long-distance transport to O_3 concentration was calculated as 36%, 25%, and 39%, respectively. Long-distance transport seemed to play a more significant role in the SIA formation, accounting for 56% of SIA concentration. Moreover, the calculation results of the relative incremental reactivity (RIR) showed that both O_3 and SIA formation were mainly affected by NO_x and VOCs emissions during the process of long-distance transport. The observed unexpectedly high contribution of long-distance transport to O_3 and SIA formation suggests that more extensive regional joint prevention and control policies on NO_x and VOCs emissions are warranted to mitigate secondary air pollution.

1. Introduction

Ozone (O_3) and fine particle ($PM_{2.5}$) pollution have become major environmental problems and aroused widespread concern in China (Zhu et al., 2023). In recent years, the Chinese government has implemented a series of measures such as the Clean Air Action Plan (2013–2017) (http://www.gov.cn/zwgk/2013-09/12/content_2486773.htm) and the Blue Sky Protection Campaign (2018–2020) (http://www.gov.cn/zhengce/content/2018-07/03/content_5303158.htm) to reduce pollution. Although $PM_{2.5}$ pollution control has made remarkable achievements, O_3 pollution has intensified (Dang and Liao, 2019; Zhai et al., 2019; Wang et al., 2022b). Serious regional $PM_{2.5}$ and O_3 episodes still occur frequently, especially in the major cities of China, e.g., Beijing, Shanghai, Guangzhou and Qingdao (Zhang et al., 2021c; Chen et al., 2020; Gao et al., 2020; Wang et al., 2022a; Zhang et al., 2021b). A better understanding of the causes of O_3 and $PM_{2.5}$ episodes is an important step toward developing efficient control strategies against O_3 and $PM_{2.5}$ pollution.

O_3 a secondary pollutant, is mainly produced by the photochemical reactions of volatile organic compounds (VOCs) and nitrogen oxides ($NO_x = NO + NO_2$). In addition to the local production, O_3 concentration might also be affected by other regions delivering either O_3 itself or its precursors (Sun et al., 2019; Wang et al., 2017a, 2017b; Xue et al., 2014). A lot of field and model studies also explored the contribution of

* Corresponding author.
** Corresponding author.
E-mail addresses: hliubin@sdu.edu.cn (L. Huang), xuelikun@sdu.edu.cn (L. Xue).

https://doi.org/10.1016/j.apgeochem.2023.105729
Received 19 March 2023; Received in revised form 12 June 2023; Accepted 22 June 2023
Available online 24 June 2023

local photochemical formation and regional transport to O_3 concentration (Wang et al., 2019; Lyu et al., 2019; Gong et al., 2020; Zhang et al., 2021e). Wang et al. (2019) revealed the spatial differences in the contribution of regional transport to O_3 pollution. They found that local production dominated O_3 pollution in the Pearl River Delta and Beijing-Tianjin-Hebei regions, but the transboundary O_3 pollution in the Yangtze River Delta was significant. Gong et al. (2020) performed a quantification study about the transport of O_3 from central eastern to north China with the GEOS-Chem model, revealing that O_3 transport from central eastern China can contribute 36% of the enhanced O_3 concentration in North China. Our previous work also traced the sources of O_3 pollution at Mount Tai by integrating field observation and model simulation (Zhang et al., 2021e). Using the Lagrangian photochemical trajectory model (LPTM), which was developed on the structure of the PTM model by combining the Lagrangian backward trajectory model and the MCM box model (Derwent and Jenkin, 1991; Hough and Derwent, 1987), we found that the contribution of transport from outside of North China Plain (NCP) to O_3 concentration was ~26%. Although regional transport is verified to be the major source of O_3 concentration, there remains the question of whether this enhancement is contributed by the input from surrounding areas or air mass coming from a longer distance. Moreover, this may have a significant impact on the formulation of detailed pollution prevention and control measures. Therefore, it is essential to further understand the effects of long-distance transport on O_3 pollution and their driving forces.

Secondary inorganic aerosols (SIA), including nitrate (NO_3^-), sulfate (SO_4^{2-}) and ammonium (NH_4^+), are critical drivers of severe haze in China and account for 30%–60% of the total fine particulate matter ($PM_{2.5}$) mass during the haze events in China (Huang et al., 2014; Zhao et al., 2013). Gaseous sulfur dioxide (SO_2) and ammonia (NH_3) are well-known as the precursors of sulfate and ammonium in the atmosphere (Fu et al., 2017; Guo et al., 2019; Zhang et al., 2021a). Previous studies revealed that the homogeneous reaction of NO_2 with OH radicals during the daytime and the heterogeneous reactions of NO_3 and N_2O_5 during the nighttime is the main formation pathways of NO_3^- (Brown and Stutz, 2012; Wang et al., 2009). For nitrate chemistry, in addition to the abundance of its precursors, atmospheric oxidants (such as OH radicals and O_3) generated by the reaction of NO_x and VOCs are also key influencing factors. Given the same precursors contained, regional transport may also play an important role in producing nitrate like O_3. Moreover, the successful application of the LPTM model on O_3 formation also implies that it may be feasible to quantify the contribution of regional transport to the formation of nitrate and other SIA using the LPTM model as well.

Therefore, in this study, we carried out a three-year continuous field management (from September 2018 to August 2021) on monitoring the concentration of O_3 and $PM_{2.5}$ as well as their precursors in Qingdao, one of the major cities in China. The seasonal and interannual variations of O_3 and $PM_{2.5}$ was studied. Furthermore, we also developed the LPTM model and used it to investigate the role of regional transport, particularly for long-distance transport, that plays in O_3 and $PM_{2.5}$ episodes and elucidate the detailed mechanism.

2. Methods

2.1. Sample collection

The three-year field observation campaign was performed from September 2018 to August 2021 in Qingdao, China. As shown in Fig. 1, the observation site is located on a six-floor roof of a building about 15 m above the ground in Qingdao (120.67°E, 36.35°N). During the campaign, the concentrations of $PM_{2.5}$, O_3, NO, NO_2, SO_2 and CO, as well as meteorological parameters (i.e., relative humidity (RH), temperature, pressure and wind speed) were obtained from the ambient air quality monitoring station of Qingdao. VOCs concentrations were measured by online gas chromatography-mass spectrometry (TT24xr, Makers, UK; GC–MS, Thermo Scientific, USA). The particle number spectrum was recorded by Scanning Mobility Particle Sizer (SMPS, GRIMM, Germany) and Wide-range Particle Sizer (WPS, MSP, USA). $PM_{2.5}$ samples were collected by a medium volume air sampler (TH-150A, Wuhan Tianhong Instrument, China) and the water-soluble inorganic components in $PM_{2.5}$ were detected by the ion chromatography (ICS-600, Dionex, USA). More details about the sample collection and measurement method can be seen in our previous studies (Zhang et al., 2021d; Liu et al., 2021; Yang et al., 2007; Zhu et al., 2021).

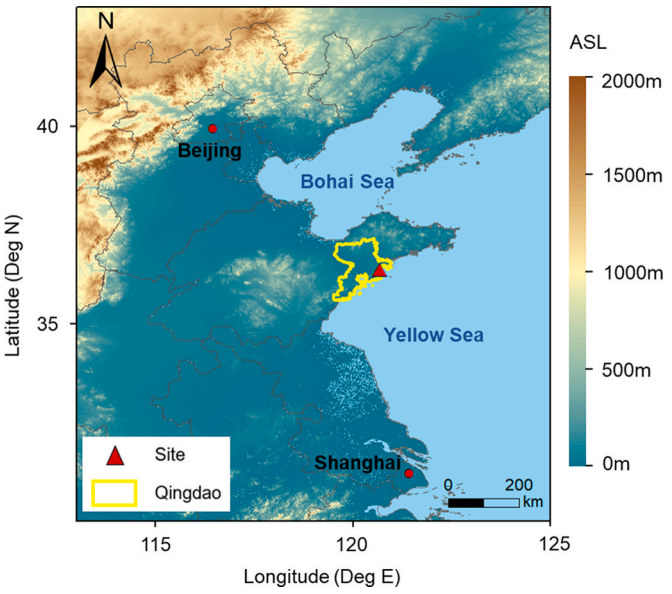

Fig. 1. Map of Qingdao and the sampling site (36.35°N, 120.67°E). The sampling site is about 1.3 km away from the coastline in Qingdao.

2.2. Lagrangian Photochemical Trajectory Model

The main sources and mechanisms for O_3 and SIA formation in the regional transport process were analyzed by the Lagrangian Photochemical Trajectory Model (LPTM) (Zhang et al., 2021e), which was built based on the coupling of the Lagrangian backward trajectory model with the chemical box model.

Both single backward trajectories and clusters were obtained using the HYSPLIT model (Draxler and Hess, 1998; Stein et al., 2015). The 3-day backward trajectories of selected 16 O_3 episode days (defined as the daily maximum 8 h average O_3 exceeded 75 ppbv) and 28$PM_{2.5}$ episode days (defined as the 24 h average $PM_{2.5}$ exceeded 75 μg m^{-3}) was calculated once a day, with an ending at an altitude of 100 m above the observation site. The trajectories of above the O_3 episodes and $PM_{2.5}$ episodes were classified into a few major clusters using a built-in clustering analysis tool within the HYSPLIT model, respectively. The Global DATA Assimilation System (GDAS) archived data (1°) was used to drive the HYSPLIT model. Real-time meteorological parameters (temperature and RH) and planetary boundary layer (PBL) for the single backward trajectories were obtained along with the backward trajectories.

The LPTM consists of five major modules: input, initialization, physical, chemical, and output. The input module was used to read grid emission rates of primary pollutants data (CO, SO_2, NH_3, NO_x and non-methane VOCs (NMVOCs)) and meteorological data (temperature and RH). Three types of primary emission sources including anthropogenic, biogenic and biomass burning emissions were considered. The data of anthropogenic emissions were obtained from the MEIC inventory (Multi-resolution Emission Inventory for China; 0.25° × 0.25°; monthly resolution in 2017; http://www.meicmodel.org/; Li et al., 2014). The data of biogenic emissions were obtained from the inventory developed by the group of Jintai Lin (Global high-resolution natural emissions;

0.25° × 0.3125°; monthly resolution in 2017; www.pku-atmos-acm.org/; Weng et al., 2020). And biomass burning emissions data were provided by the Global Fire Emission Database (0.25° × 0.25°; monthly resolution in 2019 and 2020; http://www.globalfiredata.org/; Akagi et al., 2011). For anthropogenic and biological sources, when the air mass trajectory was below PBL, the primary pollutants were considered as well mixed and their emission rate was calculated; otherwise, their emission rate was set to zero. Biomass combustion sources were assumed to be well mixed within 2000 m. The initialization module was used to set the initial concentrations of major pollutants (CO, SO_2, NH_3, NO_x, O_3, NMVOCs, NO_3^-, SO_4^{2-}, NH_4^+ and Cl^- etc.), meteorological parameters and other related parameters, including H^+, liquid water content (LWC) and particle radius. For major pollutants, if the air mass trajectory was below the PBL, the initial major pollutants were set using the median of the observed value in Qingdao on the first day of the trajectory. Otherwise, the 10th percentile of the observation data was used. Due to the lack of observed NH_3, the initial concentration of NH_3 was obtained from other studies (Meng et al., 2014; Pan et al., 2018; Xiang et al., 2022). The meteorological parameters were initialized using the data obtained along with the backward trajectories. H^+ and LWC calculated by ISORROPIA–II were initialized using the median value and the particle radius was initialized using the observed median radius. Physical and chemical modules incorporated complex physical and chemical processes. The physical processes majorly contain regional transport, variation of solar radiation intensity, dilution, and dry deposition. The chemical process was simulated based on RACM-CAPRAM multiphase chemical mechanism. RACM-CAPRAM was constructed by the gas-phase chemical mechanism of RACM2 coupled with the liquid-phase chemical mechanism of CAPRAM2.4 (Ervens et al., 2003; Goliff et al., 2013). The gas-particle partitioning reaction in the RACM-CAPRAM multiphase chemical mechanism was parameterized according to the method proposed by Schwartz (1986). In the model simulation, the primary pollutants emission rate and meteorological parameters were read at the time resolution of 1 h, and then the complex chemical reaction and physical process of these pollutants were carried out. Finally, the output module outputted the selected species concentrations and reaction rates.

Based on the model simulation, we quantified the contribution of local production and regional transport to O_3 and SIA concentration in the O_3 and $PM_{2.5}$ episodes in Qingdao. In addition, sensitivity analysis was performed to decouple the relationship between the regional transport and the precursors of O_3 or SIA. In this study, two major O_3 precursor groups (i.e., NO_x and VOCs) and four SIA precursor groups (i.e., NH_3, NO_x SO_2 and VOCs) were considered.

3. Results and discussion

3.1. Overview of filed observation

Fig. 2 shows the time series of major trace gasses (i.e., NO, NO_2, CO, SO_2, O_3, VOCs), $PM_{2.5}$ and meteorological parameters from September 2018 to August 2021in Qingdao. The mean concentrations of O_3, CO, SO_2, NO, NO_2, and $PM_{2.5}$ were measured as 38.9 ± 19.0 ppbv, 577 ± 296 ppbv, 2.60 ± 1.36 ppbv, 1.78 ± 2.29 ppbv, 9.55 ± 7.85 ppbv and 32.8 ± 34.3 μg m^{-3}, respectively. Table S1 lists the annual concentration of these compounds during the observation. It is found that there is no obvious change in the annual concentration of $PM_{2.5}$ from 2019 to

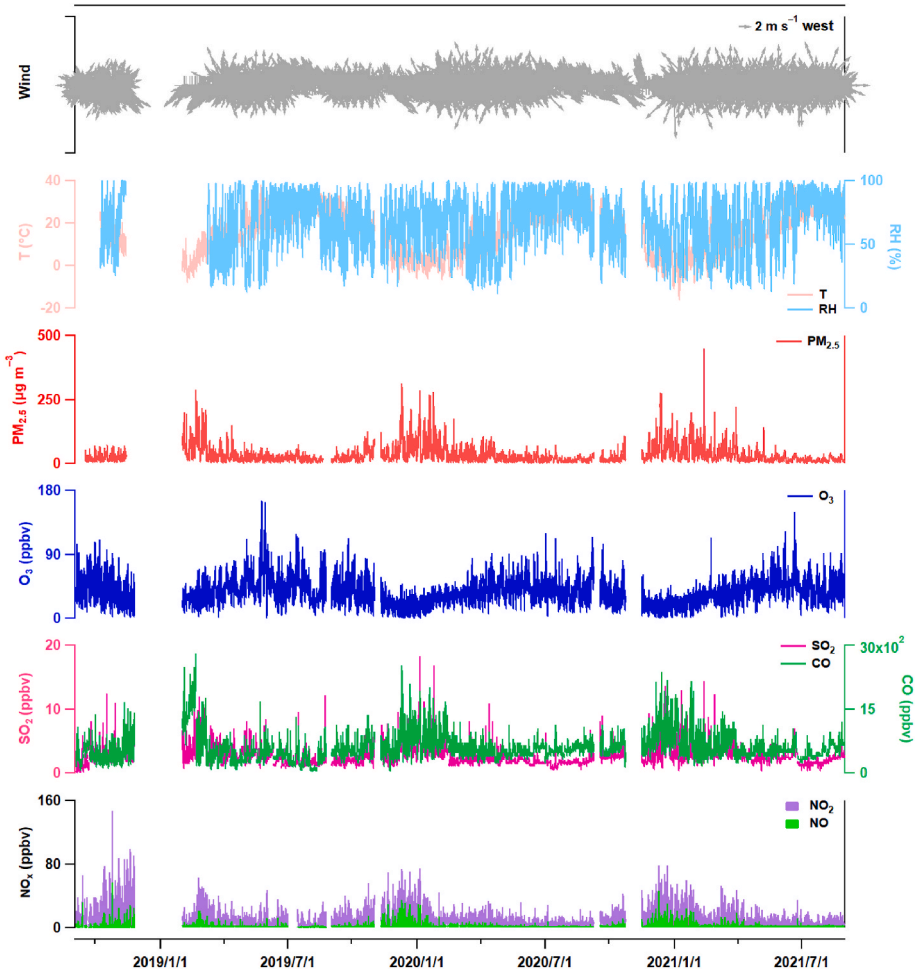

Fig. 2. Time series of pollutants and meteorological parameters from September 2018 to August 2021 in Qingdao.

2021 (2019 was defined as from September 2018 to August 2019, 2020 was defined as from September 2019 to August 2020, and 2021 was defined as from September 2020 to August 2021). The annual mean concentration of $PM_{2.5}$ from 2019 to 2021 was measured as 31.6 ± 33.4, 34.2 ± 35.8, and 32.0 ± 33.2 μg m^{-3}, respectively. The annual mean O_3 concentration from 2019 to 2021 was also measured as 44.5 ± 20.8, 35.9 ± 17.0 and 37.3 ± 18.5 ppbv, respectively. O_3 concentration decreased first and then slightly increased. This trend is also consistent with the annual variation of NO_x concentration, indicating the importance of NO_x emission reduction to O_3 pollution control. The previous study also pointed out the shift in O_3 sensitivity from the VOCs limited regime to the transitional regime in eastern China (Wang et al., 2021).

Fig. 3 displays that these pollutants exhibit strong seasonality. O_3 concentration exhibits a distinguished seasonal variation. The peak of

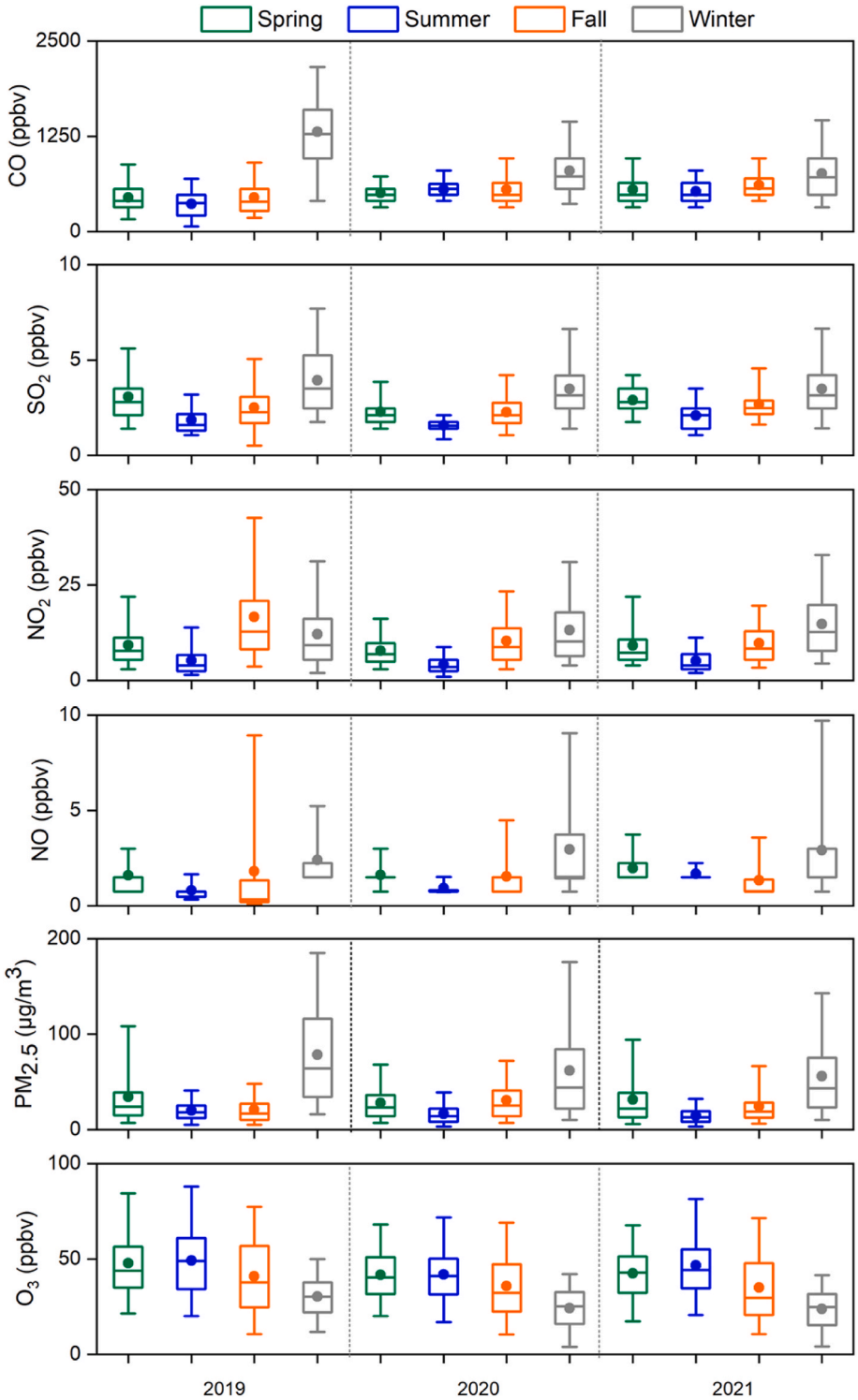

Fig. 3. Temporal variations of CO, SO_2, NO_2, NO, $PM_{2.5}$ and O_3 based on hourly measurements at the observation site from September 2018 to August 2021. The box plot provides the 5%, 25%, 50%, 75% and 95% of the data, while the dots indicate the mean concentration. (Spring: March, April, May; Summer: Jun, July, August; Fall: September, October, November; Winter: December, January, February).

seasonal mean O_3 concentration shown in summer (45.7 ± 18.6 ppbv) may be resulted from the higher temperature and stronger photochemical activity, thereby promoting O_3 production (Zhang et al., 2018). For $PM_{2.5}$, the highest (61.4 ± 51.3 μg m^{-3}) and lowest (16.9 ± 10.7 μg m^{-3}) mean seasonal concentration of $PM_{2.5}$ was observed in winter and summer, respectively. This may be attributed to the comprehensive effects of exacerbated $PM_{2.5}$ precursors emission from heating and the lower mixing layer in winter (Miao et al., 2015; Zhang et al., 2001, 2009). Consistent with the seasonal variation trend of $PM_{2.5}$, the concentrations of gaseous pollutants (CO, NO_x, and SO_2) generally peak in winter and decrease substantially in summer.

3.2. Analysis of O_3 sources

According to the Grade II standard of the Chinese Ambient Air Quality Standards (CAAQS, GB 3095-2012), the O_3 pollution was defined as the daily maximum 8 h average of O_3 concentration exceeding 75 ppbv in this study. Although annual mean O_3 concentrations decreased due to the effective control measures, we still observed 85 O_3 episodes during the whole three-year campaign. Fig. S1(a) displayed that O_3 episode days mainly occurred in summer, especially in 2019 summer, accounting for about 19% of the total O_3 episode days (16 days). As mentioned above, O_3 is a secondary pollutant produced by photochemical reactions of VOCs and NO_x (Wang et al., 2017b). In addition to the local production, O_3 concentration can also be affected by other regions delivering either O_3 itself or its precursors. Given the frequent O_3 episodes occurring in 2019 summer, a total of 16 O_3 episodes in this period were selected to study how O_3 pollution was contributed by the local formation and regional transport (hereafter called Case 1). The non-negligible effects of transportation on O_3 pollution were also verified by the results of the backward trajectories of air mass (Fig. S2). The 3-day backward trajectories indicated that air masses passed through the polluted areas (e.g., Yangtze River Delta) before arriving at the observation site during these O_3 episode days.

In this study, we employed the LPTM model to quantify the contribution of local formation and regional transport to O_3 concentration for Case 1. This model was successfully applied to quantify the contribution of regional transport and local production to O_3 concentration in Mt. Tai in our previous work (Zhang et al., 2021e). Before the quantification study, the accuracy of the O_3 concentration simulated by the LPTM model was examined. As shown in Fig. 4, the modeling LPTM concentration of O_3, O_x, NO_x and CO was in agreement with the observation data and showed a strong correlation (R^2: 0.43–0.85) with the observation data. Moreover, the relevant evaluation indicators, such as mean fractional bias (MFB) and mean fractional error (MFE), were also in line with the benchmark (MFB: 15%; MFE: 35%) recommended by the USEPA (2007) (Table S2). These results indicated that LPTM simulation results could be used for further calculation about the contribution of local production and regional transport to O_3 concentration in Qingdao.

The contributions of the local production and regional transport to O_3 concentrations were calculated by the regional O_3 formation potential (ROFP) (Zhang et al., 2021e). The ROFP of the air mass passing through a specific region can be expressed as equation (E1):

$$\mathrm{ROFP} = O_{3\ MAX} - O_{3\ MIN} \quad \text{(E1)}$$

Where O_{3MAX} refers to the maximum hourly O_3 concentration simulated by LPTM on the last day of the receptor region, and O_{3MIN} refers to the minimum hourly O_3 concentration simulated by LPTM before the appearance of O_{3MAX} in the receptor region. O_x ($O_x = O_3 + NO_2$) instead of O_3 was used to calculate ROFP to eliminate the influence of NO titration and represent a good measure of O_3 production (Jain et al., 2022). The ROFP of local (Qingdao) and other regions is calculated as 23.7 ± 28.1 and 36.4 ± 26.9 ppbv, respectively. Local production and transport can contribute to 36% and 64% of O_3 concentration in Qingdao, respectively, implying the significant influence of regional

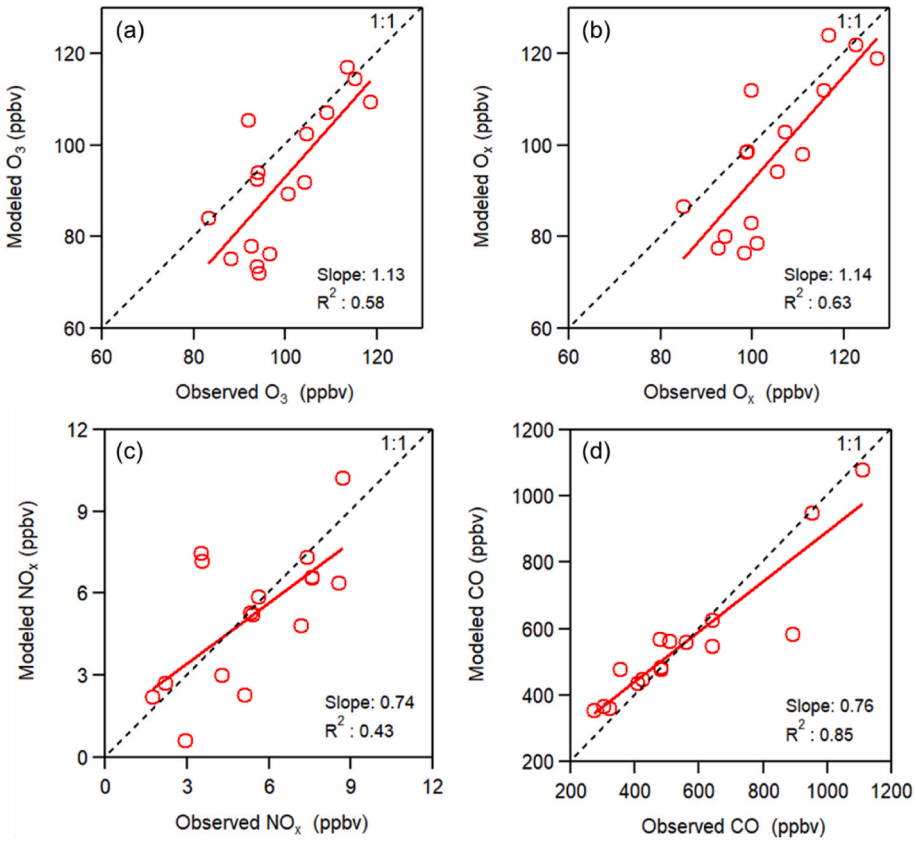

Fig. 4. Comparison of (a) O_3, (b) O_x, (c) NO_x, and (d) CO between field observations and LPTM simulations for the 16 O_3 episodes in 2019 summer.

transport on O_3 pollution in Qingdao.

We further specify the contribution of regional transport by dividing it into short-distance and long-distance transport. Short-distance transport represents the contribution of the area less than 200 km away from Qingdao (Fig. S3). Otherwise, it is called long-distance transport. The range of short-distance transport defined is approximate to the region of the Yangtze River Delta, one of the major urban agglomerations in China. As shown in Fig. 5(a), the short-distance transport contributes 25% of O_3 concentration in Case 1. The contribution of long-distance transport (39%) is 1.5 times larger than that of short-distance transport. This value is also higher than that of local production (36%), suggesting the significant role of long-distance transport in O_3 formation in Qingdao.

The detailed mechanisms for the influence of long-distance transport are further investigated. According to the results of the 3-day backward trajectories of 16 O_3 episodes, the air masses arriving in Qingdao were assembled into three clusters that mainly came from the northeast (Cluster-1), southeast (Cluster-2) and southwest (Cluster-3) of Qingdao (Fig. 6(a)). Given that NO_x and VOCs are the major precursors for O_3 formation, the relative incremental reactivity (RIR) value of NO_x and VOCs for O_3 formation was estimated in the areas where air mass clusters pass through. The RIR here is defined as the ratio of the percent decrease in the O_3 concentrations in Qingdao to the percent decrease in the emissions of the target O_3 precursors over a specific source region that can be expressed as equation (E2):

$$\mathrm{RIR}_{O_3}(\mathrm{X}) = \frac{\left[C_{O_3}(X) - C_{O_3}(X - \Delta X)\right] / C_{O_3}(X)}{\Delta X / X} \quad \text{(E2)}$$

Where C_{O_3} is the O_3 concentration in Qingdao simulated by LPTM, X represents the emission rate of the specific precursor (NO_x or VOCs); ΔX is the hypothetical change of the emission rate of X (10% in this study in accordance with the previous studies (Wang et al., 2018; Shen et al., 2021; Zheng et al., 2023)). The positive RIR values indicate that the emission reduction of such precursor inhibits the O_3 formation, and the negative values indicate the reduction of its precursor promotes O_3 formation. Fig. 6(b) shows the RIR values of O_3 affected by NO_x and VOCs over long-distance transport. Although the frequency of Cluster-3 air masses approaches 50%, NO_x and VOCs carried by Cluster-3 have a negligible impact on O_3 concentration in Qingdao. O_3 concentration seems to be pronouncedly affected by air masses from Cluster-2 air mass. These air masses from the southeast may pass through the Yangtze River Delta, where industry and ports are located, with the large emission of NO_x and VOCs. Data from the MEIC inventory shows that NO_x and VOCs emitted per unit area in the Yangtze River Delta are 4.5 and 5.2 times the national average, respectively (An et al., 2021). Therefore, the collaborative emission reduction of NO_x and VOCs, especially for the Yangtze River Delta, may be important to alleviate O_3 pollution in Qingdao.

3.3. Analysis of SIA sources

During the campaign, it was also found that there were still 80 days of $PM_{2.5}$ concentration over the Grade II CAAQS for $PM_{2.5}$ (75 μg m^{-3} for 24 h average). The highest number of $PM_{2.5}$ episode days is observed in 2020 winter, with a total of 28 days (Fig. S1(b)). It is worth noting that, among the $PM_{2.5}$ episodes, the proportion of SIA also significantly increased in addition to concentration compared to non-$PM_{2.5}$ episode days (Table 1). The concentrations of SIA comprise about half of the $PM_{2.5}$ mass in these episode days. Previous studies pointed out that regional transport can also serve as a potentially important source of SIA formation (Du et al., 2020; Lim et al., 2020; Zhong et al., 2022). The results of 3-day backward trajectories during the $PM_{2.5}$ episodes support the speculation that SIA formation in Qingdao may be related to the regional transport (Fig. S4). Thus, we also used the LPTM model to explore the role of local production and transport on SIA formation in Qingdao by selecting the $PM_{2.5}$ episodes that occurred in 2020 winter as the case (Case 2). As shown in Fig. 7, the modeling LPTM concentration of CO, SO_2, and NO_x was comparable to the observation data with strong correlations (R^2: 0.42–0.76). The relevant evaluation indicators of MFB and MFE were also in line with the benchmark (MFB: 50%; MFE: 75%) recommended by the USEPA (2007) (Table S3). The results of the uncertainties analysis indicate that the LPTM model could reproduce the increased process of SIA concentration for Case 2 and undergo further simulation.

The importance of local production and regional transport to SIA concentrations were assessed by the calculation result of the regional SIA formation potential (RSIAFP) using the equation (E3):

$$\mathrm{RSIAFP} = SIA_{MAX} - SIA_{MIN} \quad \text{(E3)}$$

Where SIA_{MAX} refers to the maximum hourly SIA concentration simulated by LPTM on the last day of the receptor region, and SIA_{MIN} refers to the minimum hourly SIA concentration simulated by LPTM before the appearance of SIA_{MAX} in the receptor region. The RSIAFP of local production and regional transport was calculated as 7.34 ± 11.45 and 31.28 ± 34.41 μg m^{-3}, respectively. The value of regional transport calculated is about four times higher than that of the local production, indicating the important contribution of regional transport to SIA concentration for Case 2. Analogously, the specific contributions from short-distance and long-distance transport were further identified. It is found that the role of long-distance transport that plays in $PM_{2.5}$ episodes seems to be more important than that in the O_3 episodes. As shown in Fig. 5(b), long-distance transport can contribute to 56% of SIA concentration, dominating the SIA formation in Qingdao. Long-distance transport also significantly contributes to the formation of SIA components, calculated as 61% for NO_3^-, 54% for NH_4^+ and 49% for SO_4^{2-}, respectively (Fig. S5).

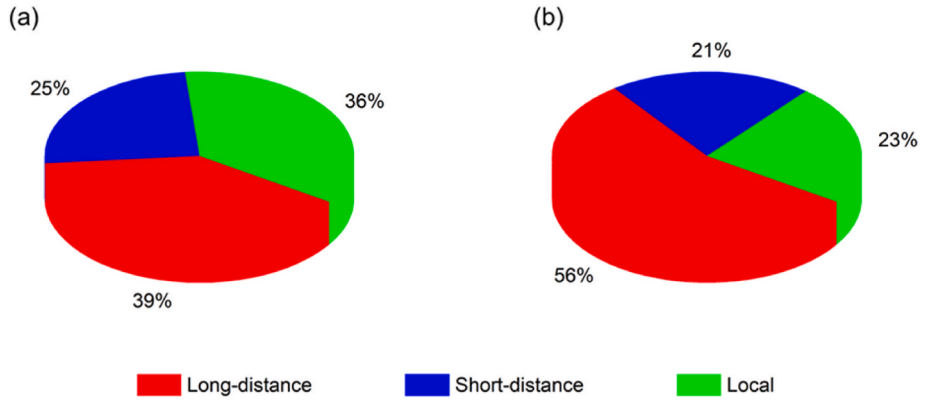

Fig. 5. Contribution ratio of local, short-distance transport and long-distance transport to the LPTM-simulated (a) O_x concentrations during the O_3 episodes in 2019 summer and (b) SIA concentrations during the $PM_{2.5}$ episodes in 2020 winter in Qingdao.

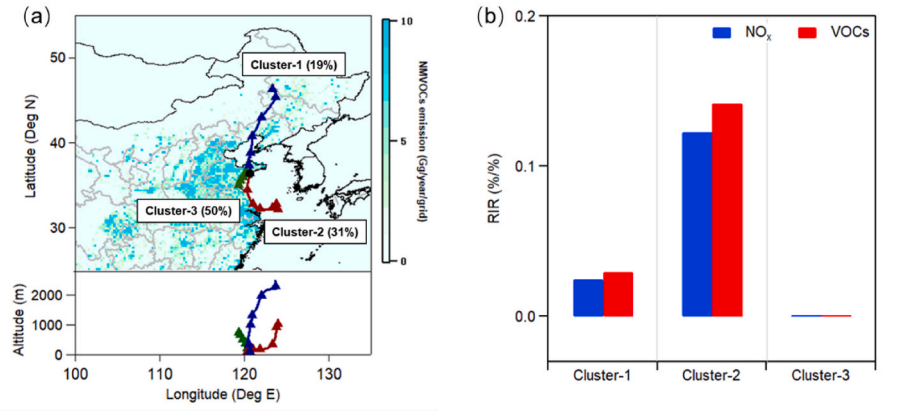

Fig. 6. (a) The 3-day backward trajectories of principle air mass clusters arriving in Qingdao during the 16 O_3 episodes. (b) RIRs of O_3 calculated at 10% of NO_x and VOCs reduction in the air mass clusters during long-distance transport.

Table 1
Concentrations of the SIA components and $PM_{2.5}$ as well as SIA/$PM_{2.5}$ ratio in $PM_{2.5}$ episodes and non-$PM_{2.5}$ episodes in the 2019 winter.

Species (μg m^{-3})	$PM_{2.5}$ episode days	non-$PM_{2.5}$ episode days	All days
$PM_{2.5}$	133.2 ± 39.8	42.3 ± 16.7	85.1 ± 54.9
SO_4^{2-}	14.05 ± 7.57	3.81 ± 2.20	8.63 ± 7.43
NO_3^-	33.10 ± 18.44	8.89 ± 7.79	20.28 ± 18.28
NH_4^+	14.92 ± 7.98	3.82 ± 3.07	9.04 ± 8.07
SIA	62.07 ± 33.31	16.51 ± 12.95	37.95 ± 33.45
SIA/$PM_{2.5}$	46% ± 21%	35% ± 15%	40% ± 19%

In analogous to O_3, RIR values of SIA are calculated to evaluate the role of its precursors (SO_2, NO_x, NH_3 and VOCs) that play during long-distance transport. Air masses can also be assembled into three clusters during the 28 $PM_{2.5}$ episode days according to the corresponding 3-day backward trajectory (Fig. 8(a)). And then, the response of LPTM-simulated SIA in Qingdao to the SIA precursors in a specific source region that air masses clusters are passed was calculated by equation (E4):

$$\mathrm{RIR}_{SIA}(X) = \frac{[C_{SIA}(X) - C_{SIA}(X-\Delta X)]/C_{SIA}(X)}{\Delta X/X} \quad \text{(E4)}$$

Where C_{SIA} is the SIA concentration in Qingdao simulated by LPTM, X represents the emission rate of the specific precursor (SO_2, NO_x NH_3 or VOCs); ΔX is the hypothetical change of the emission rate of X (10% in this study). As shown in Fig. 8(b), it was found that the reductions of SO_2 and NH_3 likely have an insignificantly important influence on SIA concentration. This may arise from the acidity of particle changes accompanying the reduction of sulfate or NH_4^+, and subsequently aid the formation of other SIA components, thereby maintaining SIA at a constant. Previous filed studies observed the enhanced particulate acidity resulted from NH_3 emission reduction, thereby facilitating the enhancement of nitrate formation by reducing $ClNO_2$ production from NO_2^+ (a product of N_2O_5 heterogeneous uptake) and Cl^- (Roberts et al., 2008; Wen et al., 2018). It is noted that SIA concentration is significantly affected by the reduction of either NO_x or VOCs. For Cluster-1 and Cluster-3 air masses, SIA formation was most sensitive to NO_x reduction (Fig. 8). NO_x emission reduction plays a double-edged role in SIA formation. On the one hand, NO_x reduction decreased the concentration of HNO_3, which is not conducive to the conversion of HNO_3 and NH_3 to particulate NH_4NO_3, resulting in the decrease of NO_3^- and NH_4^+ concentration (Wen et al., 2018). On the other hand, the reduction of NO_x can increase the concentration of O_3 and H_2O_2 and then promote the aqueous-phase formation of SO_4^{2-} (Tsimpidi et al., 2008). Although an increase in SO_4^{2-} somewhat offsets the benefit of reduced NO_3^-, NO_x reduction may still be effective in SIA concentration decrease (Fig. S6). For air masses Clusrer-2, SIA formation is most sensitive to VOCs reduction rather than NO_x. VOCs reduction could effectively reduce the concentration of atmospheric oxidants, inhibiting the formation of NO_3^-, SO_4^{2-} and NH_4^+. The high sensitivity of SIA to VOCs reduction also indicates the importance of reducing atmospheric oxidation levels for SIA and $PM_{2.5}$ pollution control in winter.

4. Conclusions

This work presents a three-year continuous observation of O_3 and $PM_{2.5}$ in Qingdao, China, from September 2018 to August 2021. It is found that both $PM_{2.5}$ and O_3 exhibit strong seasonality. $PM_{2.5}$ generally peaks in winter and decreases substantially in summer, while O_3 shows the converse trend. Furthermore, the interannual variation of $PM_{2.5}$ and

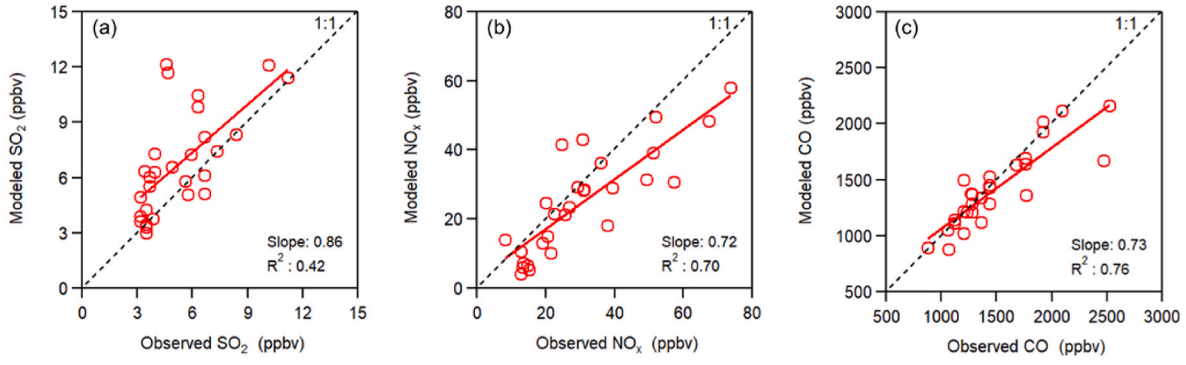

Fig. 7. Comparison of (a) SO_2, (b) NO_x and (c) CO between field observations and LPTM simulations for the 28 $PM_{2.5}$ episodes in 2020 winter.

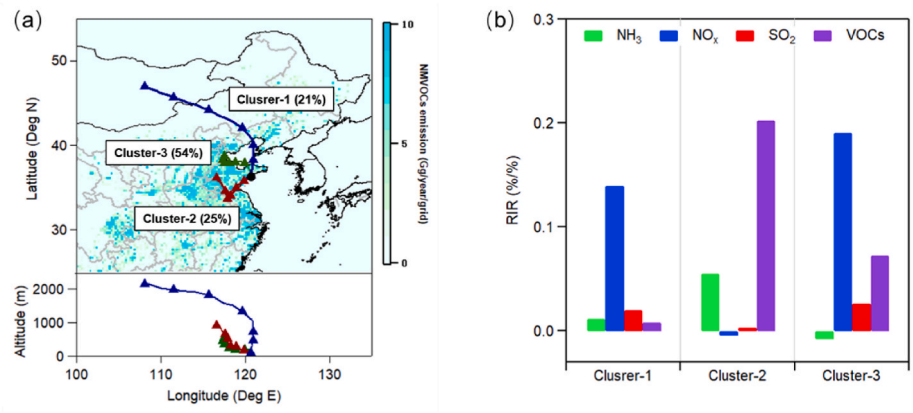

Fig. 8. (a) The 3-day backward trajectories of principle air mass clusters arriving in Qingdao during $PM_{2.5}$ episodes in 2020 winter. (b) RIRs of SIA calculated at 10% of different precursors (NH_3, NO_x, SO_2, and VOCs) reduction in the air mass clusters during long-distance transport.

O_3 concentrations was also investigated. The annual mean concentrations of O_3 and $PM_{2.5}$ were 35.9–44.5 ppbv and 31.6–34.2 μg m^{-3}, respectively. Analysis of the interannual variation of O_3 and $PM_{2.5}$ concentration indicates the effective control measures for $PM_{2.5}$ and O_3 pollution in Qingdao in recent years. However, we still observed 85 O_3 episodes and 80 $PM_{2.5}$ episodes during the whole observation, suggesting the importance of understanding the causes of O_3 and $PM_{2.5}$ episodes to further improve air quality.

Based on observational data, we employed the LPTM to quantify the contribution of local photochemical formation and regional transport to O_3 concentration during O_3 episodes. The average contribution of local production, short-distance transport, and long-distance transport to O_3 concentration was calculated as 36%, 25%, and 39%, respectively, during the O_3 episodes in 2019 summer. This result suggests the potentially important role of long-distance transport in O_3 concentration increased when O_3 episodes occurred. We also performed for the first time to apply LPTM to investigate the sources of SIA given that they are also secondary pollutants and their formation may also be affected by the local production and regional transport. A higher contribution of long-distance transport to SIA formation was observed (56%). Long-distance transport may play a previously underrated role in O_3 and $PM_{2.5}$ pollution in Qingdao. Furthermore, the analysis of the relative incremental reactivity (RIR) shows that both O_3 and SIA formation are mainly affected by NO_x and VOCs emissions during the process of long-distance transport. These findings highlight the importance of regional transport, particularly for long-distance transport, for O_3 and $PM_{2.5}$ production, and provide valuable insight into the formulation of control measures for O_3 and $PM_{2.5}$ in a typical Chinese major city. Although the results of selected cases in this study prove the significant contribution of regional transport to O_3 and SIA in Qingdao, the temporal variation of regional transport contribution to O_3 and SIA in Qingdao is unclear. In the future, we will continue to conduct observations in Qingdao to explore the influence of regional transport on the long-term change trend of O_3 and SIA in Qingdao.

Declaration of competing interest

The authors declare that they have no known competing financial interests or personal relationships that could have appeared to influence the work reported in this paper.

Data availability

No data was used for the research described in the article.

Acknowledgements

This study was supported by the National Natural Science Foundation of China (42061160478 and 42075094) and the Outstanding Young Scholar of the Natural Science Foundation of Shandong Province, China (Overseas) (grant no. 2022HWYQ-010).

Appendix A. Supplementary data

Supplementary data to this article can be found online at https://doi.org/10.1016/j.apgeochem.2023.105729.

References

Akagi, S.K., Yokelson, R.J., Wiedinmyer, C., Alvarado, M.J., Reid, J.S., Karl, T., Crounse, J.D., Wennberg, P.O., 2011. Emission factors for open and domestic biomass burning for use in atmospheric models. Atmos. Chem. Phys. 11 (9), 4039–4072. https://doi.org/10.5194/acp-11-4039-2011.

An, J.Y., Huang, Y.W., Huang, C., Wang, X., Yan, R.S., Wang, Q., Wang, H.L., Jing, S.A., Zhang, Y., Liu, Y.M., Chen, Y., Xu, C., Qiao, L.P., Zhou, M., Zhu, S.H., Hu, Q.Y., Lu, J., Chen, C.H., 2021. Emission inventory of air pollutants and chemical speciation for specific anthropogenic sources based on local measurements in the Yangtze River Delta region, China. Atmos. Chem. Phys. 21 (3), 2003–2025. https://doi.org/10.5194/acp-21-2003-2021.

Brown, S.S., Stutz, J., 2012. Nighttime radical observations and chemistry. Chem. Soc. Rev. 41, 6405–6447. https://doi.org/10.1039/C2CS35181A.

Chen, Y.Y., Bai, Y., Liu, H.T., Alatalo, J.M., Jiang, B., 2020. Temporal variations in ambient air quality indicators in Shanghai municipality, China. Sci. Rep. 10, 11350 https://doi.org/10.1038/s41598-020-68201-0.

Dang, R.J., Liao, H., 2019. Radiative forcing and health impact of aerosols and ozone in China as the consequence of Clean Air Actions over 2012-2017. Geophys. Res. Lett. 46 (21), 12511–12519. https://doi.org/10.1029/2019GL084605.

Derwent, R.G., Jenkin, M.E., 1991. Hydrocarbons and the long-range transport of ozone and pan across Europe. Atmos. Environ., Part A 25 (8), 1661–1678. https://doi.org/10.1016/0960-1686(91)90025-3.

Draxler, R.R., Hess, G.D., 1998. An overview of the HYSPLIT_4 modelling system for trajectories, dispersion and deposition. Aust. Meteorol. Mag. 47, 295–308.

Du, H.Y., Li, J., Wang, Z.F., Dao, X., Guo, S., Wang, L.L., Ma, S.L., Wu, J.B., Yang, W.Y., Chen, X.S., Sun, Y.L., 2020. Effects of regional transport on haze in the North China Plain: transport of precursors or secondary inorganic aerosols. Geophys. Res. Lett. 47 (14), e2020GL087461 https://doi.org/10.1029/2020GL087461.

Ervens, B., George, C., Williams, J.E., Buxton, G.V., Salmon, G.A., Bydder, M., Wilkinson, F., Dentener, F., Mirabel, P., Wolke, R., Herrmann, H., 2003. CAPRAM 2.4 (MODAC mechanism): an extended and condensed tropospheric aqueous phase mechanism and its application. J. Geophys. Res. Atmos. 108 https://doi.org/10.1029/2002JD002202.

Fu, X., Wang, S.X., Xing, J., Zhang, X.Y., Wang, T., Hao, J.M., 2017. Increasing ammonia concentrations reduce the effectiveness of particle pollution control achieved via SO_2 and NO_x emissions reduction in east China. Environ. Sci. Technol. Lett. 4 (6), 221–227. https://doi.org/10.1021/acs.estlett.7b00143.

Gao, Y., Shan, H.Y., Zhang, S.Q., Sheng, L.F., Li, J.P., Zhang, J.X., Ma, M.C., Meng, H., Luo, K., Gao, H.W., Yao, X.H., 2020. Characteristics and sources of $PM_{2.5}$ with focus on two severe pollution events in a coastal city of Qingdao, China. Chemosphere 247, 125861. https://doi.org/10.1016/j.chemosphere.2020.125861.

Goliff, W.S., Stockwell, W.R., Lawson, C.V., 2013. The regional atmospheric chemistry mechanism, version 2. Atmos. Environ. 68, 174–185. https://doi.org/10.1016/j.atmosenv.2012.11.038.

Gong, C., Liao, H., Zhang, L., Yue, X., Dang, R.J., Yang, Y., 2020. Persistent ozone pollution episodes in North China exacerbated by regional transport. Environ. Pollut. 265, 115056 https://doi.org/10.1016/j.envpol.2020.115056.

Guo, Z.Y., Guo, Q.J., Chen, S.L., Zhu, B., Zhang, Y.L., Yu, J.H., Guo, Z.B., 2019. Study on pollution behavior and sulfate formation during the typical haze event in Nanjing with water soluble inorganic ions and sulfur isotopes. Atmos. Res. 217, 198–207. https://doi.org/10.1016/j.atmosres.2018.11.009.

Hough, A.M., Derwent, R.G., 1987. Computer modelling studies of the distribution of photochemical ozone production between different hydrocarbons. Atmos. Environ. 21 (9), 2015–2033. https://doi.org/10.1016/0004-6981(87)90163-6.

Huang, R.J., Zhang, Y.L., Bozzetti, C., Ho, K.F., Cao, J.J., Han, Y.M., Daellenbach, K.R., Slowik, J.G., Platt, S.M., Canonaco, F., Zotter, P., Wolf, R., Pieber, S.M., Bruns, E.A., Crippa, M., Ciarelli, G., Piazzalunga, A., Schwikowski, M., Abbaszade, G., Schnelle-Kreis, J., Zimmermann, R., An, Z.S., Szidat, S., Baltensperger, U., Haddad, I.E., Prévôt, A.S.H., 2014. High secondary aerosol contribution to particulate pollution during haze events in China. Nature 514, 218–222. https://doi.org/10.1038/nature13774.

Jain, C.D., Ratnam, M.V., Madhavan, B.L., Sindhu, S., Kumar, A.H., 2022. Impact of regional transport on total O_x (NO_2+ O_3) concentrations observed at a tropical rural location. Atmos. Pollut. Res. 13 (5), 101408 https://doi.org/10.1016/j.apr.2022.101408.

Li, M., Zhang, Q., Streets, D.G., He, K.B., Cheng, Y.F., Emmons, L.K., Huo, H., Kang, S.C., Lu, Z., Shao, M., Su, H., Yu, X., Zhang, Y., 2014. Mapping Asian anthropogenic emissions of non-methane volatile organic compounds to multiple chemical mechanisms. Atmos. Chem. Phys. 14 (11), 5617–5638. https://doi.org/10.5194/acp-14-5617-2014.

Lim, Y.B., Seo, J., Kim, J.Y., Kim, Y.P., Jin, H.C., 2020. Local formation of sulfates contributes to the urban haze with regional transport origin. Environ. Res. Lett. 15 (8), 084034 https://doi.org/10.1088/1748-9326/ab83aa.

Liu, Y.H., Shen, H.Q., Mu, J.S., Li, H.Y., Chen, T.S., Yang, J., Jiang, Y., Zhu, Y.J., Meng, H., Dong, C., Wang, W.X., Xue, L.K., 2021. Formation of peroxyacetyl nitrate (PAN) and its impact on ozone production in the coastal atmosphere of Qingdao, North China. Sci. Total Environ. 778, 146265 https://doi.org/10.1016/j.scitotenv.2021.146265.

Lyu, X.P., Wang, N., Guo, H., Xue, L.K., Jiang, F., Zeren, Y.Z., Cheng, H.R., Cai, Z., Han, L. H., Zhou, Y., 2019. Causes of a continuous summertime O_3 pollution event in Jinan, a central city in the North China Plain. Atmos. Chem. Phys. 19 (5), 3025–3042. https://doi.org/10.5194/acp-19-3025-2019.

Meng, Z.Y., Zhang, R.J., Lin, W.L., Jia, X.F., Yu, X.M., Yu, X.L., Wang, G.H., 2014. Seasonal variation of ammonia and ammonium aerosol at a background station in the Yangtze River Delta Region, China. Aerosol Air Qual. Res. 14, 756–766. https://doi.org/10.4209/aaqr.2013.02.0046.

Miao, Y.C., Liu, S.H., Zheng, Y.J., Wang, S., Liu, Z.X., Zhang, B.H., 2015. Numerical study of the effects of Planetary Boundary Layer structure on the pollutant dispersion within built-up areas. J. Environ. Sci. 32, 168–179. https://doi.org/10.1016/j.jes.2014.10.025.

Pan, Y.P., Tian, S.L., Zhao, Y.H., Zhang, L., Zhu, X.Y., Gao, J., Huang, W., Zhou, Y.B., Song, Y., Zhang, Q., Wang, Y.S., 2018. Identifying ammonia hotspots in China using a national observation network. Environ. Sci. Technol. 52 (7), 3926–3934. https://doi.org/10.1021/acs.est.7b05235.

Roberts, J.M., Osthoff, H.D., Brown, S.S., Ravishankara, A.R., 2008. N_2O_5 oxidizes chloride to Cl_2 in acidic atmospheric aerosol. Science 321 (5892), 1059. https://doi.org/10.1126/science.1158777.

Schwartz, S.E., 1986. Mass-transport considerations pertinent to aqueous phase reactions of gases in liquid-water clouds. Chemistry of Multiphase Atmospheric Systems 415–417. https://doi.org/10.1007/978-3-642-70627-1_16.

Shen, H.Q., Liu, Y.H., Zhao, M., Li, J., Zhang, Y.N., Yang, J., Jiang, Y., Chen, T.S., Chen, M., Huang, X.B., Li, C.L., Guo, D.L., Sun, X.Y., Xue, L.K., Wang, W.X., 2021. Significance of carbonyl compounds to photochemical ozone formation in a coastal city (Shantou) in eastern China. Sci. Total Environ. 764, 144031 https://doi.org/10.1016/j.scitotenv.2020.144031.

Stein, A.F., Draxler, R.R., Rolph, G.D., Stunder, B.J.B., Cohen, M.D., Ngan, F., 2015. NOAA'S HYSPLIT atmospheric transport and dispersion modeling system. Bull. Am. Meteorol. Soc. 96 (12), 2059–2077. https://doi.org/10.1175/BAMS-D-14-00110.1.

Sun, L., Xue, L.K., Wang, Y.H., Li, L.L., Lin, J.T., Ni, R.J., Yan, Y.Y., Chen, L.L., Li, J., Zhang, Q.Z., Wang, W.X., 2019. Impacts of meteorology and emissions on summertime surface ozone increases over central eastern China between 2003 and 2015. Atmos. Chem. Phys. 19 (3), 1455–1469. https://doi.org/10.5194/acp-19-1455-2019.

Tsimpidi, A.P., Karydis, V.A., Pandis, S.N., 2008. Response of fine particulate matter to emission changes of oxides of nitrogen and anthropogenic volatile organic compounds in the Eastern United States. J AIR WASTE MANAGE 58 (11), 1463–1473. https://doi.org/10.3155/1047-3289.58.11.1463.

USEPA, 2007. USEPA: Guidance on the Use of Models and Other Analyses for Demonstrating Attainment of Air Quality Goals for Ozone, $PM_{2.5}$ and Regional Haze. United States Environmental Protection Agency, NC. EPA-454/B-07e002.

Wang, H.W., Gao, Y., Sheng, L.F., Wang, Y.H., Zeng, X.R., Kou, W.B., Ma, M.C., Cheng, W.X., 2022a. The impact of meteorology and emissions on surface ozone in Shandong Province, China, during Summer 2014—2019. Int. J. Environ. Res. Publ. Health 19 (11), 6758. https://doi.org/10.3390/ijerph19116758.

Wang, M.Y., Yim, Steve H.L., Wong, D.C., Ho, K.F., 2019. Source contributions of surface ozone in China using an adjoint sensitivity analysis. Sci. Total Environ. 662, 385–392. https://doi.org/10.1016/j.scitotenv.2019.01.116.

Wang, R., Xu, X.B., Jia, S.H., Ma, R.S., Ran, L., Deng, Z.Z., Lin, W.L., Wang, Y., Ma, Z.Q., 2017a. Lower tropospheric distributions of O_3 and aerosol over Raoyang, a rural site in the North China Plain. Atmos. Chem. Phys. 17 (6), 3891–3903. https://doi.org/10.5194/acp-17-3891-2017.

Wang, T., Xue, L.K., Brimblecombe, P., Lam, Y.F., Li, L., Zhang, L., 2017b. Ozone pollution in China: a review of concentrations, meteorological influences, chemical precursors, and effects. Sci. Total Environ. 575, 1582–1596. https://doi.org/10.1016/j.scitotenv.2016.10.081.

Wang, T., Xue, L.K., Feng, Z.Z., Dai, J.N., Zhang, Y.N., Tan, Y., 2022b. Ground-level ozone pollution in China: a synthesis of recent findings on influencing factors and impacts. Environ. Res. Lett. 17, 063003 https://doi.org/10.1088/1748-9326/ac69fe.

Wang, W.N., van der A, R., Ding, J.Y., van Weele, M., Cheng, T.H., 2021. Spatial and temporal changes of the ozone sensitivity in China based on satellite and ground-based observations. Atmos. Chem. Phys. 21 (9), 7253–7269. https://doi.org/10.5194/acp-21-7253-2021.

Wang, X.F., Zhang, Y.P., Chen, H., Yang, X., Chen, J.M., Geng, F.H., 2009. Particulate nitrate formation in a highly polluted urban area: a case study by single-particle mass spectrometry in Shanghai. Environ. Sci. Technol. 43 (9), 3061–3066. https://doi.org/10.1021/es8020155.

Wang, Y., Guo, H., Zou, S.C., Lyu, X.P., Ling, Z.H., Cheng, H.R., Zeren, Y.Z., 2018. Surface O_3 photochemistry over the South China Sea: application of a near-explicit chemical mechanism box model. Environ. Pollut. 234, 155–166. https://doi.org/10.1016/j.envpol.2017.11.001.

Wen, L., Xue, L.K., Wang, X.F., Xu, C.H., Chen, T.S., Yang, L.X., Wang, T., Zhang, Q.Z., Wang, W.X., 2018. Summertime fine particulate nitrate pollution in the North China Plain: increasing trends, formation mechanisms and implications for control policy. Atmos. Chem. Phys. 18 (15), 11261–11275. https://doi.org/10.5194/acp-18-11261-2018.

Weng, H.J., Lin, J.T., Martin, R., Millet, D.B., Jaeglé, L., Ridley, D., Keller, C., Li, C., Du, M.X., Meng, J., 2020. Global high-resolution emissions of soil NO_x, sea salt aerosols, and biogenic volatile organic compounds. Sci. Data 7, 148. https://doi.org/10.1038/s41597-020-0488-5.

Xiang, Y.K., Dao, X., Gao, M., Lin, Y.C., Cao, F., Yang, X.Y., Zhang, Y.L., 2022. Nitrogen isotope characteristics and source apportionment of atmospheric ammonium in urban cities during a haze event in Northern China Plain. Atmos. Environ. 269, 118800 https://doi.org/10.1016/j.atmosenv.2021.118800.

Xue, L.K., Wang, T., Gao, J., Ding, A.J., Zhou, X.H., Blake, D.R., Wang, X.F., Saunders, S. M., Fan, S.J., Zuo, H.C., Zhang, Q.Z., Wang, W.X., 2014. Ground-level ozone in four Chinese cities: precursors, regional transport and heterogeneous processes. Atmos. Chem. Phys. 14 (23), 13175–13188. https://doi.org/10.5194/acp-14-13175-2014.

Yang, L.X., Wang, D.C., Cheng, S.H., Wang, Z., Zhou, Y., Zhou, X.H., Wang, W.X., 2007. Influence of meteorological conditions and particulate matter on visual range impairment in Jinan, China. Sci. Total Environ. 383, 164–173. https://doi.org/10.1016/j.scitotenv.2007.04.042.

Zhai, S.X., Jacob, D.J., Wang, X., Shen, L., Li, K., Zhang, Y.Z., Gui, K., Zhao, T.L., Liao, H., 2019. Fine particulate matter ($PM_{2.5}$) trends in China, 2013-2018: separating contributions from anthropogenic emissions and meteorology. Atmos. Chem. Phys. 19 (16), 11031–11041. https://doi.org/10.5194/acp-19-11031-2019.

Zhang, G., Xu, H.H., Qi, B., Du, R.G., Gui, K., Wang, H.L., Jiang, W.T., Liang, L.L., Xu, W. Y., 2018. Characterization of atmospheric trace gases and particulate matter in Hangzhou, China. Atmos. Chem. Phys. 18 (3), 1705–1728. https://doi.org/10.5194/acp-18-1705-2018.

Zhang, L.M., Gong, S.L., Padro, J., Barrie, L., 2001. A size-segregated particle dry deposition scheme for an atmospheric aerosol module. Atmos. Environ. 35 (3), 549–560. https://doi.org/10.1016/S1352-2310(00)00326-5.

Zhang, Q., Streets, D.G., Carmichael, G.R., He, K.B., Huo, H., Kannari, A., Klimont, Z., Park, I.S., Reddy, S., Fu, J.S., Chen, D., Duan, L., Lei, Y., Wang, L.T., Yao, Z.L., 2009. Asian emissions in 2006 for the NASA INTEX-B mission. Atmos. Chem. Phys. 9 (14), 5131–5153. https://doi.org/10.5194/acp-9-5131-2009.

Zhang, R., Han, Y.H., Shi, A.J., Sun, X.S., Yan, X., Huang, Y.H., Wang, Y., 2021a. Characteristics of ambient ammonia and its effects on particulate ammonium in winter of urban Beijing, China. Environ. Sci. Pollut. Res. 28, 62828–62838. https://doi.org/10.1007/s11356-021-14108-w.

Zhang, X., Li, H., Wang, X.Z., Zhang, Y.J., Bi, F., Wu, Z.H., Liu, Y.H., Zhang, H., Gao, R., Xue, L.K., Zhang, Q.Z., Chen, Y.Z., Chai, F.H., Wang, W.X., 2021b. Heavy ozone pollution episodes in urban Beijing during the early summertime from 2014 to 2017: implications for control strategy. Environ. Pollut. 285 (15), 117162 https://doi.org/10.1016/j.envpol.2021.117162.

Zhang, Y.N., Xue, L.K., Carter, W.P.L., Pei, C.L., Chen, T.S., Mu, J.S., Wang, Y.J., Zhang, Q.Z., Wang, W.X., 2021c. Development of ozone reactivity scales for volatile organic compounds in a Chinese megacity. Atmos. Chem. Phys. 21 (14), 11053–11068. https://doi.org/10.5194/acp-21-11053-2021.

Zhang, Y., Yang, L.X., Bie, S.J., Zhao, T., Huang, Q., Li, J.S., Wang, P.C., Wang, Y.M., Wang, W.X., 2021d. Chemical compositions and the impact of sea salt in atmospheric PM_1 and $PM_{2.5}$ in the coastal area. Atmos. Res. 250, 105323 https://doi.org/10.1016/j.atmosres.2020.105323.

Zhang, Y.N., Xue, L.K., Li, H.Y., Chen, T.S., Mu, J.S., Dong, C., Sun, L., Liu, H.D., Zhao, Y., Wu, D., Wang, X.F., Wang, W.X., 2021e. Source apportionment of regional ozone pollution observed at Mount Tai, North China: application of Lagrangian Photochemical Trajectory Model and implications for control policy. J. Geophys. Res. Atmos. 126 (6), e2020JD033519 https://doi.org/10.1029/2020JD033519.

Zhao, P.S., Dong, F., He, D., Zhao, X.J., Zhang, X.L., Zhang, W.Z., Yao, Q., Liu, H.Y., 2013. Characteristics of concentrations and chemical compositions for $PM_{2.5}$ in the region of Beijing, Tianjin, and Hebei, China. Atmos. Chem. Phys. 13 (9), 4631–4644. https://doi.org/10.5194/acp-13-4631-2013.

Zheng, Z.S., Li, K.W., Xu, B., Dou, J.P., Li, L.M., Zhang, G.T., Li, S.J., Geng, C.M., Yang, W., Azzi, M., Bai, Z.P., 2023. O_3–precursor relationship over multiple patterns

of timescale: a case study in Zibo, Shandong Province, China. Atmos. Chem. Phys. 23 (4), 2649–2665. https://doi.org/10.5194/acp-23-2649-2023.

Zhong, H.B., Huang, R.J., Lin, C.S., Xu, W., Duan, J., Gu, Y.F., Huang, W., Ni, H.Y., Zhu, C.S., You, Y., Wu, Y.F., Zhang, R.J., Ovadnevaite, J., Ceburnis, D., O'Dowd, C. D., 2022. Measurement report: on the contribution of long-distance transport to the secondary aerosol formation and aging. Atmos. Chem. Phys. 22 (14), 9513–9524. https://doi.org/10.5194/acp-22-9513-2022.

Zhu, T., Tang, M.J., Gao, M., Bi, X.H., Cao, J.J., Che, H.Z., Chen, J.M., Ding, A.J., Fu, P. Q., Gao, J., Gao, Y., Ge, M.F., Ge, X.L., Han, Z.W., He, H., Huang, R.J., Huang, X., Liao, H., Liu, C., Liu, H., Liu, J.G., Liu, S.C., Lu, K.D., Ma, Q.X., Nie, W., Shao, M., Song, Y., Sun, Y.L., Tang, X., Wang, T., Wang, T.J., Wang, W.G., Wang, X.M., Wang, Z.F., Yin, Y., Zhang, Q., Zhang, W.J., Zhang, Y.L., Zhang, Y.H., Zhao, Y., Zheng, M., Zhu, B., Zhu, J., 2023. Recent progress in atmospheric chemistry research in China: establishing a theoretical framework for the "Air Pollution Complex". Adv. Atmos. Sci. https://doi.org/10.1007/s00376-023-2379-0.

Zhu, Y.J., Xue, L.K., Gao, J., Chen, J.M., Li, H.Y., Zhao, Y., Guo, Z.X., Chen, T.S., Wen, L., Zheng, P.G., Shan, Y., Wang, X.F., Wang, T., Yao, X.H., Wang, W.X., 2021. Increased new particle yields with largely decreased probability of survival to CCN size at the summit of Mt. Tai under reduced SO_2 emissions. Atmos. Chem. Phys. 21 (2), 1305–1323. https://doi.org/10.5194/acp-21-1305-2021.